

Phase diagram of the ferroelectric-relaxor $(1-x)\text{PbMg}_{1/3}\text{Nb}_{2/3}\text{O}_3$ - $x\text{PbTiO}_3$

B. Noheda, D. E. Cox, and G. Shirane

Department of Physics, Brookhaven National Laboratory, Upton, NY 11973, USA.

Z.-G. Ye, and J. Gao

Department of Chemistry, Simon Fraser University, Burnaby, BC, V5A 1S6, Canada.

(Dated: October 30, 2018)

Synchrotron x-ray powder diffraction measurements have been performed on unpoled ceramic samples of $(1-x)\text{Pb}(\text{Mg}_{1/3}\text{Nb}_{2/3})\text{O}_3$ - $x\text{PbTiO}_3$ (PMN- x PT) with $30\% \leq x \leq 39\%$ as a function of temperature around the morphotropic phase boundary (MPB), which is the line separating the rhombohedral and tetragonal phases in the phase diagram. The experiments have revealed very interesting features previously unknown in this or related systems. The sharp and well-defined diffraction profiles observed at high and intermediate temperatures in the cubic and tetragonal phases, respectively, are in contrast to the broad features encountered at low temperatures. These peculiar characteristics, which are associated with the monoclinic phase of M_C -type previously reported by Kiat et al and Singh et al., can only be interpreted as multiple coexisting structures with M_C as the major component. An analysis of the diffraction profiles has allowed us to properly characterize the PMN- x PT phase diagram and to determine the stability region of the monoclinic phase, which extends from $x = 31\%$ to $x = 37\%$ at 20 K. The complex landscape of observed phases points to an energy balance between the different PMN- x PT phases which is intrinsically much more delicate than that of related systems such as $\text{PbZr}_{1-x}\text{Ti}_x\text{O}_3$ or $(1-x)\text{PbZn}_{1/3}\text{Nb}_{1/3}\text{O}_3$ - $x\text{PbTiO}_3$. These observations are in good accord with an optical study of $x = 33\%$ by Xu et al., who observed monoclinic domains with several different polar directions coexisting with rhombohedral domains, in the same single crystal.

PACS numbers:

I. INTRODUCTION

Solid solutions of the relaxor-ferroelectrics $(1-x)\text{Pb}(\text{Mg}_{1/3}\text{Nb}_{2/3})\text{O}_3$ - $x\text{PbTiO}_3$ and $(1-x)\text{Pb}(\text{Zn}_{1/3}\text{Nb}_{2/3})\text{O}_3$ - $x\text{PbTiO}_3$, known as PMN- x PT and PZN- x PT, respectively, are under active consideration for a new generation of electromechanical devices. When properly oriented, they have piezoelectric coefficients which are the highest yet reported, with electromechanical deformations one order-of-magnitude larger than those of conventional high piezoelectric PbZrO_3 - PbTiO_3 (PZT) ceramics [1, 2]. The exceptional electromechanical properties of these lead oxide-based solid solutions have long been known to be related to the nearly vertical phase boundary between the rhombohedral and the tetragonal phases, the so-called morphotropic phase boundary (MPB), which is a common feature of the PbMeO_3 - PbTiO_3 systems [3, 4, 5].

However, the origin of this unusual behavior remained unknown until recently, when a monoclinic phase was observed around the MPB of PZT, in between the rhombohedral and tetragonal phases [6, 7]. The monoclinic phase in PZT, with space group C_m , has the unique axis b_m along the [110] direction, and a unit cell that is doubled with respect to the primitive cubic one and rotated 45° about the c -axis with respect to it. We designate this monoclinic phase as M_A -type, following the notation of Vanderbilt and Cohen, who in a recent theoretical study derived for the first time a region of stability for ferroelectric monoclinic perovskites by an extension of the

classic Devonshire-Landau expansion of the free energy to eighth-order [8]. Diffraction experiments with an electric field applied in-situ [9] together with first-principles calculations [10] on PZT ceramics have demonstrated a direct link between the M_A phase and the high electromechanical deformations in PZT due to rotation of the polarization between the [111] and [001] directions. This fact explains some other studies in which an enhancement of the piezoelectric properties of [001]-oriented rhombohedral PZT was reported [11, 12].

First-principles calculations [13] have also shown that the anomalously high strain values observed in rhombohedral PZN- x PT crystals under a [001]-electric field [1] can be attributed to polarization rotation from the rhombohedral [111] to the tetragonal [001] polar axis. Diffraction experiments with an electric field applied in-situ [14, 15] have permitted the direct observation of such polarization rotation paths, and have shown that for rhombohedral PZN-8PT, which has a composition very close to the MPB, a *different* monoclinic phase (M_C in the notation of ref. [8]) is induced when an electric field is applied along the [001] direction. The M_C phase has the P_m space group, with the unique axis b_m oriented along the pseudo-cubic [010] direction. With increasing electric field, the M_C phase becomes less distorted and approaches tetragonal symmetry but when the field is decreased to zero, an orthorhombic (O) phase is reached, similar to that of BaTiO_3 , which can be viewed as an M_C phase with $a_m = c_m$ [14]. The appearance of this irreversibly-induced O phase in PZN-8PT suggested that an orthorhombic phase would probably exist close by in

this region of the phase diagram. Shortly afterwards, x-ray powder diffraction experiments [16, 17] did in fact reveal the existence of such an O phase in a narrow composition region ($8% < x < 11%$) between the rhombohedral (R) and tetragonal (T) phases in the PZN-xPT phase diagram. The O phase can be regarded as being very close in energy to the M_C phase for the following two reasons; first, a very small electric field is enough to induce the O- M_C transformation [14] and, second, one of the four PZN-9%PT samples studied by Uesu et al. [18] showed M_C symmetry rather than O.

The MPB phases of the piezoelectric system PMN-xPT [5, 19] have not been extensively studied until the last two years, during which a series of papers on this material have appeared. PMN-33%PT single crystals poled along the [011] direction appear to be orthorhombic [20], while X-ray diffraction experiments have shown that a PMN-35%PT crystal poled along the [001] directions has M_A -type monoclinic symmetry, similar to that of PZT [21]. This latter work also reports that unpoled PMN-35%PT single crystals are purely rhombohedral, in contrast to previous optical microscopy studies of crystals of the same nominal composition which reported that they display a complicated pattern of rhombohedral and tetragonal domains [22]. Very recently, fascinating domain patterns, arising from different monoclinic phases with different polarization directions, have been observed by Xu et al. in a PMN-33%PT crystal [23]. In addition, both neutron [24] and x-ray [25] powder diffraction measurements have revealed the existence of a monoclinic phase of M_C -type, in PMN-35%PT at low temperatures, and in PMN-34%PT at room temperature, respectively. All these results indicate that the behaviour of PMN-xPT around the MPB is very complicated and requires more systematic studies to be properly understood.

In the present work we report a high-resolution synchrotron x-ray powder diffraction study on PMN-xPT ceramic samples of several compositions as a function of temperature around the MPB. An intermediate monoclinic phase of M_C type has been observed in agreement with previous reports [24, 25]. However, in contrast to these latter results, it has been found that the monoclinic phase does not exist as a single phase in any of the samples studied. The present study has allowed us to determine the region of stability of the intermediate phase and to construct a new phase diagram for PMN-xPT.

II. EXPERIMENTAL

Samples of $(1-x)\text{PbMg}_{1/3}\text{Nb}_{2/3}\text{O}_3-x\text{PbTiO}_3$ with $x=0.30, 0.31, 0.33, 0.35, 0.37$ and 0.39 (hereafter designated xPT, with x in %) were synthesized using the two-step columbite precursor technique [26]. The starting reagents were oxide powders with purities better than 99.9%. In the first step, a mixture of MgO and Nb_2O_5 containing a 15.5 wt% excess of MgO over the 1:1 stoichiometric proportions was thoroughly ground in

ethanol and cold-pressed. The excess amount of MgO was added in order to compensate for subsequent weight losses at high temperatures as determined from a previous DTA/TG analysis. The pellet was dried at 80°C and calcined at 1100°C for 12h to form pure MgNb_2O_6 of columbite structure. In the second step, this precursor powder was mixed with PbO and TiO_2 in the appropriate proportions and a 2 wt% excess of PbO added to compensate for the evaporation losses during the calcining and sintering processes. Each composition was thoroughly ground and calcined at 900°C for 4h to form the perovskite phase. The calcined powders were reground with the addition of a few drops of polyvinyl alcohol (PVA) and cold-pressed into pellets about 3 mm thick and 15 mm in diameter, which were first heated to 650°C in an open Pt crucible for 1h to drive off the PVA, and then sintered at 1200°C for 4h in an alumina crucible to form highly densified ceramics. The light yellow surfaces of the ceramic pellets were polished with fine diamond paste and ultrasonically cleaned. X-ray diffraction patterns obtained on a laboratory diffractometer with $\text{Cu K}\alpha$ confirmed the formation of perovskite-type phases with no evidence of any impurities.

Synchrotron x-ray powder diffraction measurements were performed at beamline X7A at the Brookhaven National Synchrotron Light Source on several different occasions. In each case a double-crystal channel-cut Si (111) monochromator was used in combination with a Ge (220) analyzer and a scintillation detector. The wavelength was set to $\approx 0.7 \text{ \AA}$ and calibrated with a Si reference standard. With this configuration, the angular resolution is better than 0.01° . In most cases the data were collected directly from the ceramic pellets in Bragg-Brentano geometry by carrying out step-scans at 0.005 or 0.01° intervals over selected angular regions while the sample was rocked over a few degrees to improve powder averaging. This type of scan provides good counting rates but can result in incorrect intensity ratios if significant preferred orientation is present in the pellets. However, the peak positions and hence the derived unit cell parameters are not affected by this problem. Temperature dependence measurements, between 20 and 500K, were performed with the samples loaded in a closed-cycle cryostat. A further set of measurements was made at room temperature on capillary samples which were rotated at about 1 Hz during data collection. Such data are free from preferred-orientation effects, but suffer from the disadvantage that the counting rates are quite slow. For this purpose, a small piece of each pellet was carefully crushed and sieved, and the resulting 325-400 mesh fraction (about $38\text{-}44 \mu\text{m}$) loaded into a thin glass-walled capillary of nominal diameter 0.2 mm [16]. In most cases scans were carried out over narrow angular regions centered about the six pseudocubic reflections (100), (110), (111), (200), (220) and (222), from which it is possible to determine unambiguously the crystal symmetry within the limits of the instrumental resolution, together with the corresponding lattice parameters and any zero offset

if present. For the data analysis, the individual reflection profiles were fitted to a pseudo-Voigt function appropriately corrected for asymmetry [27] with intensity, peak position, peak-width (FWHM) and mixing parameter as variables. When appropriate, the peak widths and mixing parameters were constrained to be the same for all the peaks in a clump. Additional peaks were added based on the difference patterns, the relative intensities and the goodness-of-fit residuals. Compared to the standard Rietveld technique of profile-matching, in which the full diffraction pattern is fitted without a structural model, the advantage of this procedure is that it does not require any assumptions about the phases to be included, how the FWHM and mixing parameters vary as a function of 2θ , and how to allow for anisotropic broadening, when neighboring peaks have significantly different widths. We have found that this is a fairly common effect in PbO-based perovskite systems, and is likely to occur when one or more of the lattice parameters is more sensitive to compositional fluctuations than the others. If overlooked, anisotropic broadening can be mistakenly interpreted as a lower-symmetry structure in a profile-matching analysis.

Some information about the microstructure and compositional fluctuations in the samples can be obtained from Williamson-Hall plots [28] of the peak widths, which can be used to provide estimates of the mean coherence length, L , and fluctuations in the d-spacings, $\Delta d/d$. The observed values of $\Delta d/d$ in the cubic phase are consistent with long-range compositional fluctuations in the samples of typically $\pm 1\%$ (FWHM), based on the lattice parameters reported by Noblanc et al.[19] for compositions in the range 25-40PT.

III. TEMPERATURE DEPENDENCE

The temperature evolution of the lattice parameters for 30PT and 39PT is shown in Fig 1. These two compositions are located to the left and right sides, respectively, of the MPB in the PMN-xPT phase diagram, and the Curie temperatures, T_C , are shown as vertical dotted lines. The determination of T_C , which is usually made from dielectric measurements, is difficult in this case due to the broadness of the dielectric constant peak. In this paper the T_C values have been adapted from those of Noblanc et al. [19] as the average of the two temperatures, T_m (maximum) and T_d (depoling), obtained from dielectric measurements on poled samples, which produce better-defined dielectric anomalies. Below their respective T_C 's of about 400 K and 450 K, 39PT is tetragonal down to 20K, while 30PT is first tetragonal becoming rhombohedral at about 350K [19], and remaining so down to 20 K.

The diffraction profiles around the pseudo-cubic (111), (200) and (220) diffraction peaks from 30PT and 39PT at 300K are shown in Fig. 2a and Fig. 2d, respectively, in which the least-squares fits to the data points

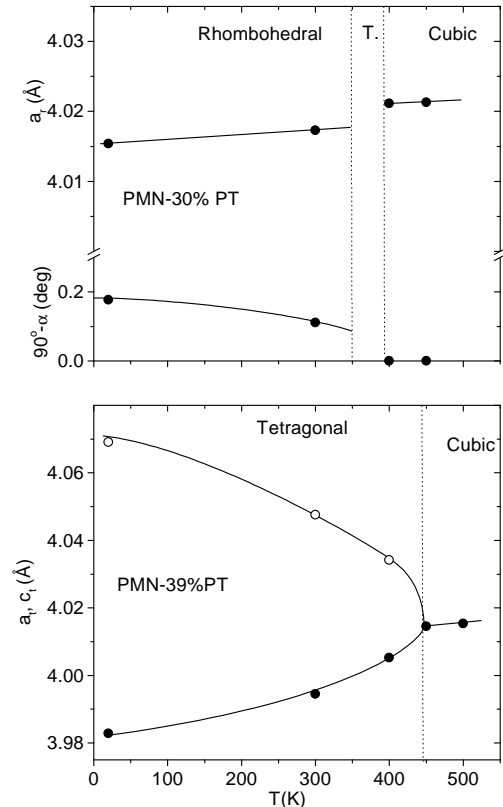


FIG. 1: Lattice parameters as a function of temperature for the PMN-30PT (top) and PMN-39PT (bottom) compositions. Dotted lines represent the respective transition temperatures as defined in the text.

are shown as solid lines and the peak positions by vertical arrows. In each case, the observed diffraction peaks show no evidence of phase coexistence; however, an analysis of the peak broadening reveals that the two compositions behave quite differently. Fig. 3 shows the respective Williamson-Hall plots [28], which have slopes of $2\Delta d/d$ and intercepts of λ/L , where L is the coherence length. While the 39PT composition shows isotropic broadening with $\Delta d/d = 9.5 \times 10^{-4}$ and a coherence length $L = 0.5 \mu\text{m}$, the 30PT composition shows highly anisotropic broadening and much smaller L values, of about $0.2 \mu\text{m}$, as shown in Fig. 3 (top). In the 30PT composition, the broadening is very small for the (hhh) peaks, with $\Delta d/d = 2.6 \times 10^{-4}$, and most pronounced for the (h00) peaks, with $\Delta d/d$ an order-of-magnitude larger. This situation is very similar to that observed in the rhombohedral phase of PZT, in which a large degree of intrinsic disorder [29] is known to exist due to the existence of local displacements of monoclinic type even though the long-range structure is rhombohedral [30].

Intermediate compositions gave considerably more complicated diffraction patterns, as can be seen in Figs.

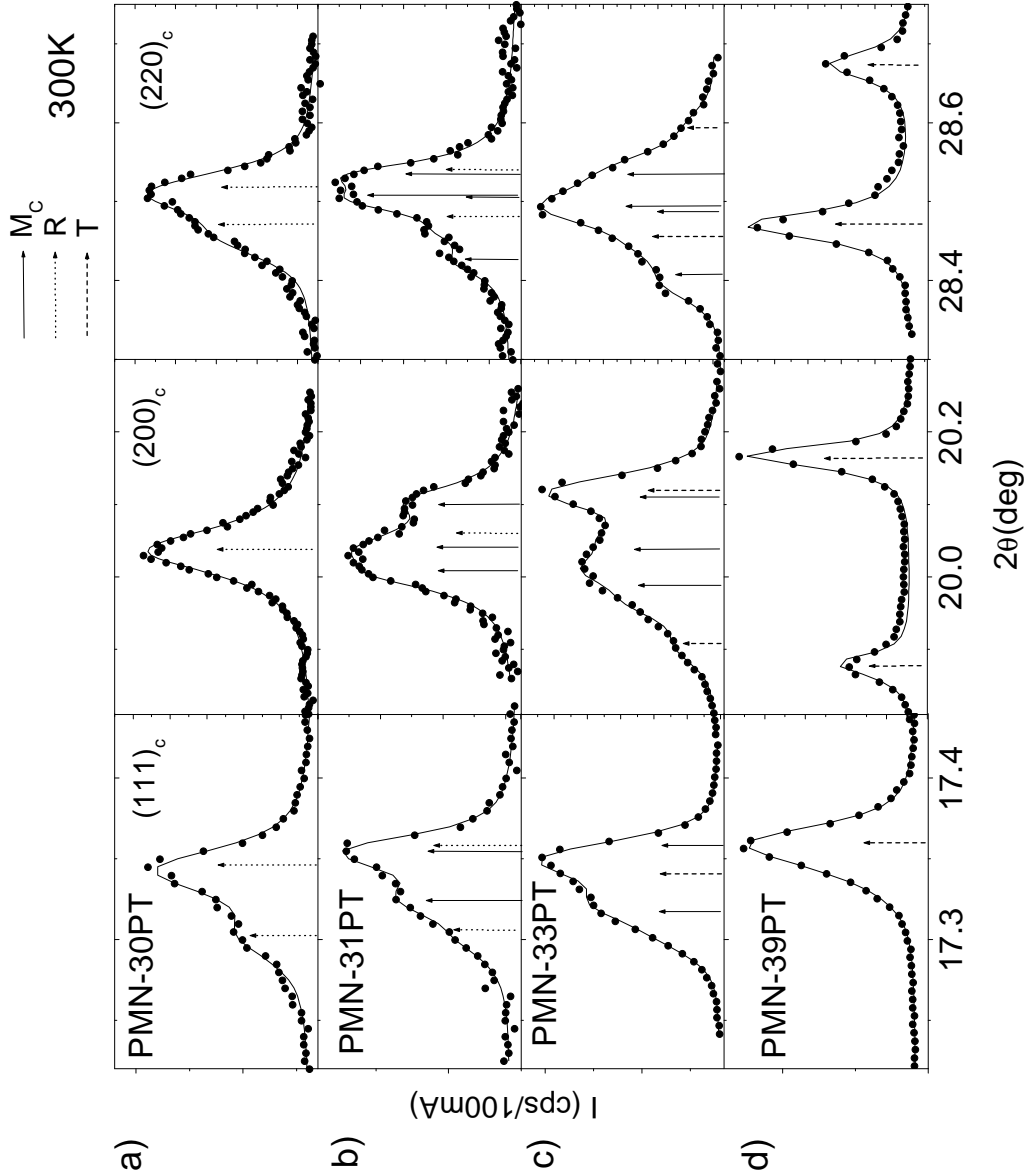


FIG. 2: Selected regions of the diffraction patterns at 300 K for (a) PMN-30PT, (b) PMN-31PT, (c) PMN-33PT and (d) PMN-39PT, corresponding to capillary samples. The solid lines are the least-squares fits to the data points and the arrows indicate the peak positions obtained from the fits.

2b and 2c for the 31PT and 33PT samples at 300K. From a detailed analysis of the peak positions and intensities of the fitted profiles, it was possible to identify a monoclinic phase of M_C -type in the 31PT, 33PT, 35PT and 37PT compositions, similar to that reported by Kiat et al.[24] and Singh et al [25]. For example, in the case of

31PT it can be seen in Fig. 2b that the profiles of the pseudo-cubic (200) and (220) reflections are distinctly different from those of 30PT shown in Fig. 2a. Various possibilities were considered to explain the observed peak positions and intensities of 31PT; in particular the lower-symmetry phases previously found in this and related

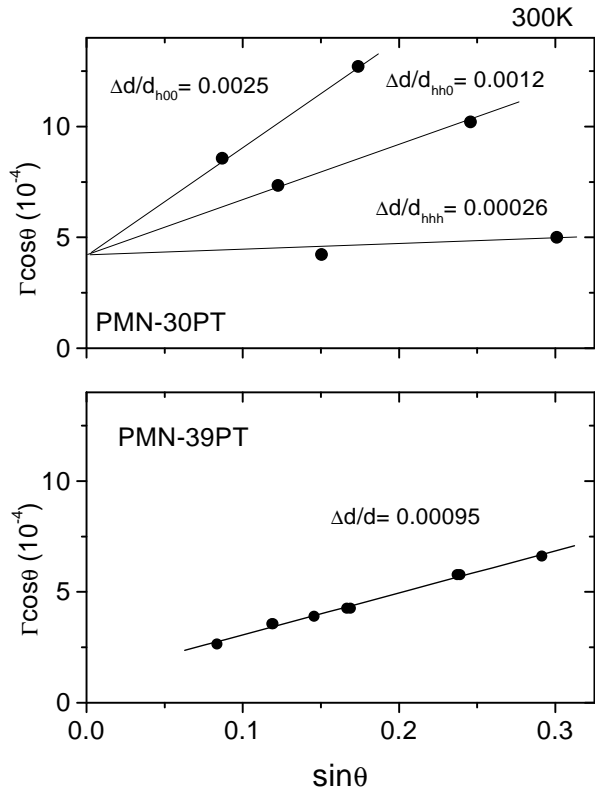


FIG. 3: Williamson-Hall plots for PMN-30PT (top) and PMN-39PT (bottom) at 300K illustrating the highly anisotropic peak broadening in PMN-30PT as compared to 39PT.

systems, i.e. orthorhombic O , monoclinic M_A and monoclinic M_C . Among these, both O and M_C are found to account quite well for most of the observed features, while M_A can be ruled out altogether. However, there are several discrepancies in the intensity ratios which can only be accounted for by the presence of a minority rhombohedral phase, with an estimated volume fraction of about 30%.

As mentioned earlier, O and M_C are closely related and very difficult to distinguish from each other, since the O phase simply represents the limiting case of the M_C phase when $a_m = c_m$. In a diffraction pattern, the difference between the two is most obvious for the pseudo-cubic (200) reflection, which would split into three peaks with roughly equal intensities for M_C , but only two peaks with a 2:1 intensity ratio for O . In the case of 31PT, it is not immediately apparent whether the broad lower-angle peak is composed of one or two peaks; however, we were able to obtain a significantly better fit with two peaks, which together with the rest of the monoclinic reflections, enabled the lattice parameters of the M_C phase to be determined with reasonable accuracy. The corresponding peak positions are indicated by solid vertical arrows in

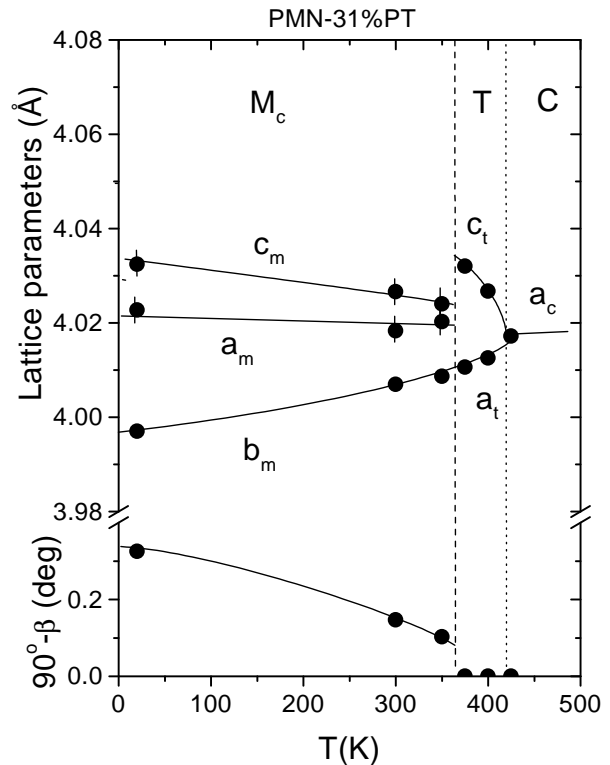


FIG. 4: Temperature evolution of the lattice parameters of PMN-31PT. The dashed line indicates the M_C - T transition temperature. The dotted line represent the T_C derived from the results of Noblanc et al. [19], as described in the text.

Fig. 2b.

The monoclinic lattice parameters of 31PT are plotted as a function of temperature in Fig. 4. At 20K, a_m and c_m are fairly well-differentiated, but they approach each other with increasing temperature and can no longer be resolved at 350K, as indicated by the error bars in Fig. 4. At the same time b_m increases and the monoclinic angle β , approaches 90° . Between 350 K and 375 K, the monoclinic phase transforms to a tetragonal one, with lattice parameters a_t and c_t . It is noteworthy that the variation between b_m and a_t is continuous at the phase transition, in striking similarity to the behavior observed for the orthorhombic phase in PZN-xPT [16, 17]. Finally, between 400K and 425K, the sample transforms into the cubic phase, consistent with the PMN-xPT phase diagram in ref. [19].

At 300K and 20K, the minority rhombohedral phase has the lattice parameters listed in Tables I and II. The corresponding peak positions at 300K are indicated by the dotted arrows in Fig. 2b. The volume fraction of the rhombohedral phase remains constant at roughly 30% up to 350 K.

TABLE I: Lattice parameters at 300K for the PMN-xPT compositions studied. The symmetries of the different phases (S) and their volume fractions (f) are indicated in the second and third columns, respectively.

x(%)	S	f(%)	a(Å)	b(Å)	c(Å)	$\alpha(=\gamma)$ (°)	β (°)
30	R	100	4.017	4.017	4.017	89.89	89.89
31	R	30	4.017	4.017	4.017	89.89	89.89
31	M	70	4.018	4.007	4.026	90	90.15
33	M	75	4.019	4.006	4.032	90	90.19
33	T	25	4.005	4.005	4.046	90	90
35	M+O	35	4.018	4.000	4.035	90	90.12
35	T	65	4.000	4.000	4.044	90	90
37	T	80	3.998	3.998	4.049	90	90
39	T	100	3.994	3.994	4.047	90	90

TABLE II: Lattice parameters at 20K for the PMN-xPT compositions studied. The symmetries of the different phases (S) and their volume fractions (f) are indicated in the second and third columns, respectively. The values have been omitted for simplicity.

x(%)	S	f(%)	a(Å)	b(Å)	c(Å)	$\alpha(=\gamma)$ (°)	β (°)
30	R	100	4.015	4.015	4.015	89.82	89.82
31	R	30	4.020	4.020	4.020	89.85	89.85
31	M	70	4.023	3.997	4.032	90	90.32
33	M	75	4.018	3.995	4.039	90	90.32
33	T	25	3.994	3.994	4.062	90	90
35	M	40	4.011	3.990	4.049	90	90.34
35	O	35	4.030	3.990	4.030	90	90.34
35	T	25	3.988	3.988	4.067	90	90
37	M	55	4.015	3.985	4.039	90	90.28
37	T	45	3.989	3.989	4.062	90	90
39	T	100	3.994	3.994	4.047	90	90

The same regions of the powder diffractogram are plotted in Fig. 2c for the 33PT composition at 300K. As in the case of 31PT, identification of the fitted peaks was based upon consideration of the R, T, M_A , M_C and O phases, both alone and in various combinations. Once again, the M_C phase was found to account satisfactorily for most of the peaks. Compared to the M_C phase of 31PT (Fig. 2b) there is a larger splitting of the three peaks in the pseudo-cubic (200) profile, corresponding to a monoclinic distortion with a greater difference between a_m and c_m , and hence more distinct from the limiting orthorhombic phase. However, as before, there were several discrepancies in the intensity ratios and clear evidence of a low-angle shoulder on the (h00) profiles which could only be explained by the presence of a minority phase, but in this case tetragonal instead of rhombohedral, with a volume fraction of about 25%. The calculated peak positions for the M_C and T phases are indicated in Fig. 2c by solid and dashed arrows respectively.

The temperature evolution of the monoclinic lattice parameters is plotted in Fig. 5, and is very similar to that of 31PT except for the larger difference between the a_m and c_m lattice parameters. Between 300-325K, the monoclinic phase transforms into a tetragonal one, which then transforms to the cubic phase between 400-

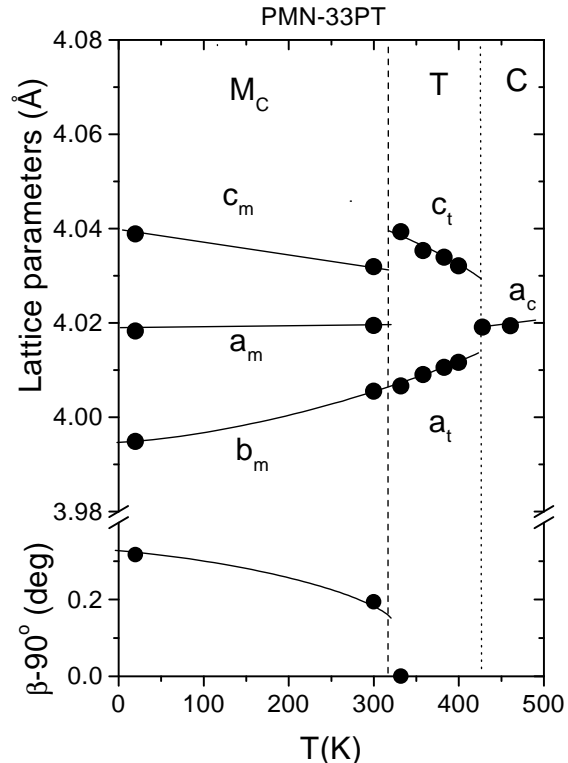


FIG. 5: Temperature evolution of the lattice parameters of PMN-33PT. The lattice parameters of the minority tetragonal phase between 20-300K (see Tables I and II) have been omitted for the sake of clarity. The dashed line indicates the M_C -T transition temperature. The dotted line represent the T_C derived from the results of Noblanc et al. [19], as described in the text.

425K, in agreement with the previously reported PMN-xPT phase diagram[19]. The volume fraction of the minority T phase is also found to be constant at about 25% over the entire temperature range in which it coexists with the M_C phase. The a_t lattice parameters at 300K and 20K are not shown in Fig. 5, but are very similar to b_m at 300K and 20K, as inferred from the overlap of the tetragonal (200) and monoclinic (020) peaks on the high-angle side of the (200) pseudo-cubic reflection (see Fig. 2c), and thus follow a continuous trend with a_t in the purely tetragonal phase at higher temperatures. c_t follows a similar continuous trend at low temperatures with c_t at higher temperatures. The tetragonal lattice parameters for 33PT at 300K and 20K are listed in Tables I and II, respectively.

The behavior observed in 35PT is more complicated. The diffraction profiles around the pseudo-cubic (200), (220) and (222) reflections are plotted in Fig. 6 for the three different symmetry regions observed as a function of temperature: the cubic phase at 450K, the tetrag-

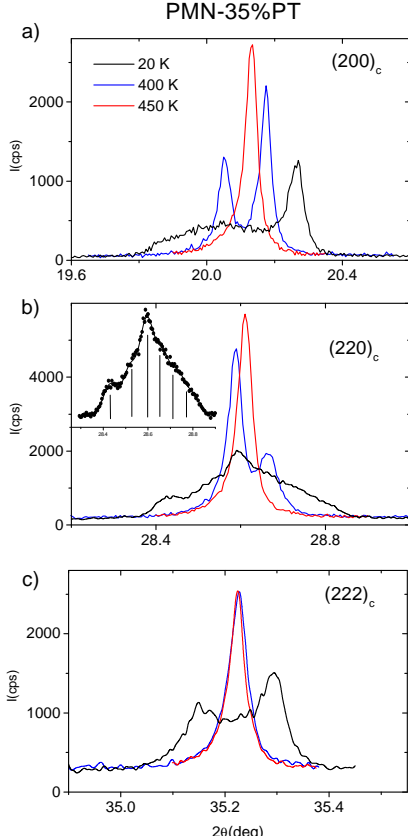


FIG. 6: (Color) Selected regions of the diffraction pattern of PMN-35PT in the cubic (450K), tetragonal (400K) and monoclinic (20K) phases. The inset shows the data points at 20K around (220), together with the fit (solid line). The peak positions obtained from the fit are indicated by the vertical lines.

onal phase at 400K, and the low temperature region at 20K. The strikingly broad features observed at low temperatures are in sharp contrast to the narrow and well-resolved peaks observed in the tetragonal and cubic phases. The high-angle peak in the (200) profile, which corresponds to the smallest lattice parameter, b_m , shifts towards higher angles and remains relatively sharp. In contrast, the intensity in the lower-angle region becomes very broad and the fitting procedure becomes accordingly more difficult. However, it is quite clear that this broadening cannot be explained simply by the existence of a second tetragonal phase. Fortunately, the (hh0) and (hhh) reflections do not show such pronounced broadening and can be fitted satisfactorily. The inset to Fig. 6b shows the experimental data points around the pseudocubic (220) reflection at 20K together with the solid line representing a six-peak fit which is in excellent agreement with the observed profile. Most of the peak positions are consistent with the coexistence of M_C and T phases, and the corresponding lattice parameters at 300K and 20 K are listed in Tables I and II, respectively. However, there

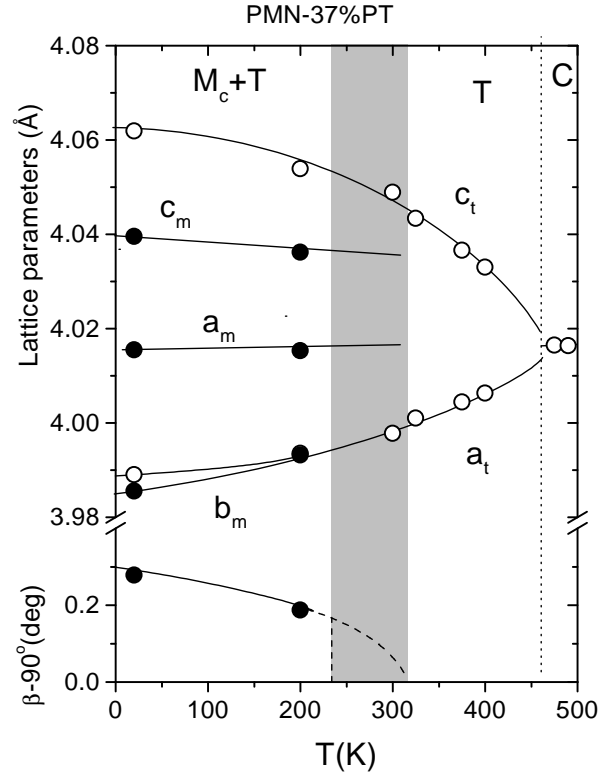


FIG. 7: Temperature evolution of the monoclinic and tetragonal lattice parameters of PMN-37PT. The temperatures interval in which the volume fraction of the monoclinic (tetragonal) phase gradually decreases (increases) is shown by the shaded region. The dotted line represent the T_C derived from the results of Noblanc et al. [19], as described in the text.

remain some significant discrepancies in the intensity ratios and also one unexplained peak in the (hh0) profiles. It turns out that these features can be accounted for very well by the presence of about 30% of a third orthorhombic (O) phase with b_m and β equal to those of M_C phase, and with $a_m = c_m$ equal to the mean value of the a_m and c_m values for M_C (see table II). At 300K, the O and M_C lattice parameters cannot be resolved.

The 37PT composition was found to be a two-phase mixture of M_C and T at low temperatures, in the approximate ratio 55:45 at both 20 K and 200K, and predominantly tetragonal at room temperature. The evolution of the lattice parameters is plotted in Fig. 7 showing for clarity only those phases with a volume fraction in excess of 40%. The volume fraction of the T phase increases from about 45% at 200K, to 80% at 300K, and is essentially 100% at 325K. Thus, as in the case of 35PT, there is a temperature interval in which the relative fractions of M_C and T phases are found to vary, which has been indicated as a shaded region in Fig. 7. The lattice parameters for the T phase at 300K and for the T

and M_C phases at 20K, are also shown in Tables I and II, respectively. Because of peak overlap, the lattice parameters of the minority monoclinic phase at 300K could not be determined. The vertical dotted line denotes the temperature of the T-C phase transition obtained, as in previously noted, from the mean values of the two temperatures reported in ref. [19].

IV. COMPOSITION DEPENDENCE

Figs. 8 and 9 show the evolution of the monoclinic phase between the rhombohedral and tetragonal regions as a function of composition at 300K and 20K, respectively. As in previous figures, only the values of the majority phases have been plotted for clarity, except for 37PT at 20K, where the volume fractions of the two phases are roughly the same. The lattice parameters reported in ref. [25] for PMN-34%PT are also plotted in Fig. 8, and are seen to be in good agreement with the present data. The region of stability of the M_C phase lies approximately between 31PT and 35PT at 300K, as reported by Singh et al[25], and it is found to extend slightly further at 20K, to 37PT. The trends in the lattice parameters show similar features at both temperatures: c_m increases and b_m decreases with increasing Ti content, while a_m and $(\beta-90^\circ)$ remain approximately constant at 300K, and decrease only slightly at 20K. Although there are relatively large errors in the determination of the lattice parameters, we can nevertheless conclude that the transition between the rhombohedral and monoclinic states is rather abrupt, as expected on symmetry grounds [31]. More unexpectedly, the transition between the monoclinic and tetragonal phases also seems to be fairly abrupt, implying that there is no continuous rotation of the polarization all the way to the tetragonal state with increasing Ti content.

Based on the above analysis, we have constructed a new phase diagram for PMN-xPT in the vicinity of the MPB, as shown in Fig. 10, in which the stability region of the M_C phase has been shaded. The solid line indicating the transition to the cubic phase has been adapted from ref. [19] as the average of the two temperatures, T_m (maximum) and T_d (depoling), proposed by Noblanc et al. [19], as previously mentioned. These transition temperatures were found to be in better agreement with our data (solid symbols) than those reported in ref. [5]. To take into account the observed phase coexistence, a dotted vertical line and horizontal dotted arrows have been included in the phase diagram, to indicate the rhombohedral ($x \lesssim 32\%$) or tetragonal ($x \gtrsim 32\%$) symmetry of the secondary phase.

V. DISCUSSION

It is interesting to note that the x-ray profiles shown in Fig. 2c for 33PT are clearly similar to those in Fig.

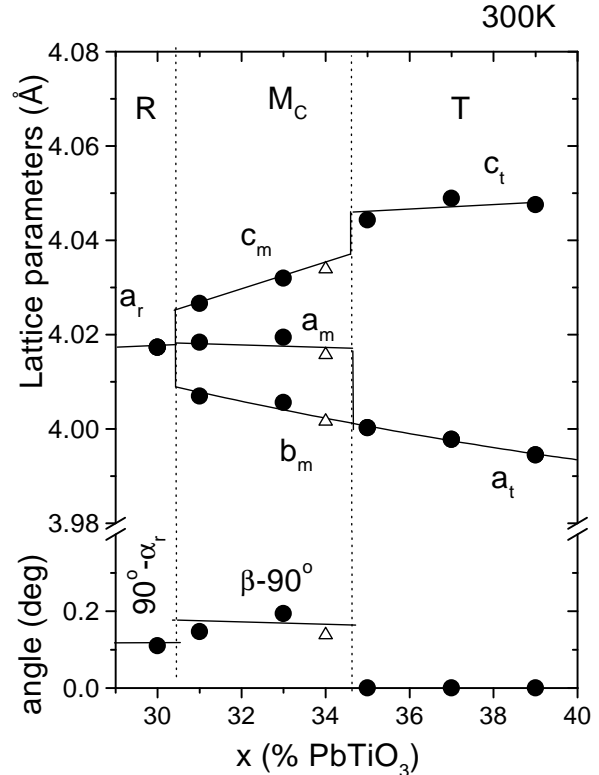


FIG. 8: Composition dependence of the lattice parameters of the majority phases in PMN-xPT around the MPB at 300K

1 of ref. [25] for 34PT. In particular, there appears to be definite evidence of a low-angle shoulder in the pseudo-cubic (200) profile, and a high-angle shoulder in the (220) profile, both of which would imply the presence of a minority tetragonal phase in the latter sample.

Recent work by Topolov [32] shows that stress fields may play a very important role at the MPB. It therefore seems plausible that local internal strain due to lattice mismatching between coexisting phases is the cause for the observed broadening of the pseudo-cubic (h00) profile in the M_C phase. This type of strain would produce a distribution of a_m and c_m lattice parameters that could explain the striking profiles seen for the 35PT sample at 20K and could include the limiting case of an orthorhombic phase for which $a_m=c_m$. The fact that such a distribution is less evident in the other profiles (see Fig. 6b-c) is because the corresponding peak splittings are defined mainly by the monoclinic angle and the average values of a_m and c_m for (hh0), and exclusively by those values for (hhh). It is also apparent that the existence of long-range compositional fluctuations about $\pm 1\%$, indicated by Williamson-Hall plots for the cubic phases, as earlier described, can only partially explain the observed distribution of monoclinic lattice parameters.

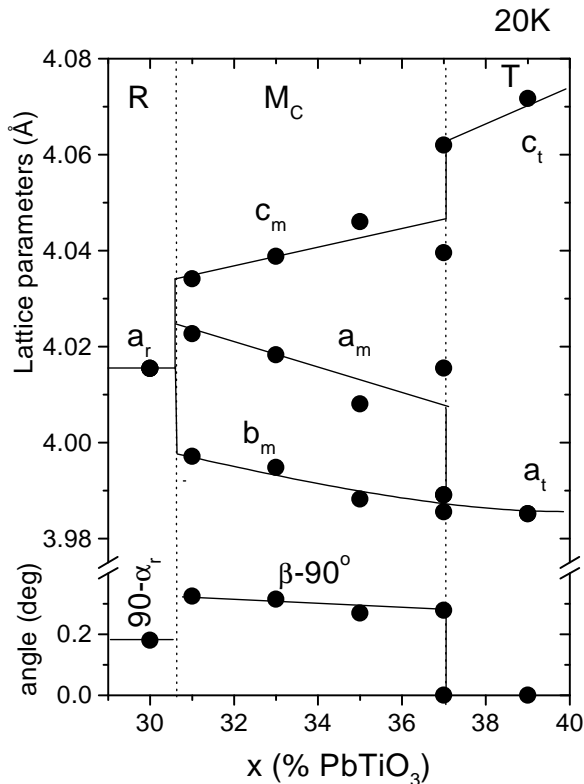


FIG. 9: Composition dependence of the lattice parameters of the majority phases in PMN-xPT around the MPB at 20K

Furthermore, in the context of the three-phase coexistence observed in 35PT at low temperatures, it is interesting to note that a degenerate point at which these three phases, T, O and M_C coexist has been predicted by Vanderbilt and Cohen [8] in an eighth-order expansion of the free energy. Although this degeneracy is actually an artifact of the model, and could be removed by considering higher-order terms in the Devonshire expansion, it is reasonable to suppose that these three phases are extremely close in energy and can in fact coexist in real systems due to internal strain, thermal fluctuations, etc. The phase diagram reported in ref. 8 may explain why the MPB of the PMN-xPT system (around the T-M_C-O "degenerate" point) is considerably more complicated than that of PZT [7] (around the T-M_A-R tricritical point) or that of PZN-xPT[17] (around the R-O-T tricritical point). Burton et al. [33] have reported a slightly lower disorder energy in PMN than in PZN. Moreover, this disorder can be expected to increase at the MPB of the PMN-xPT system due to the larger Ti content, and could also contribute to the exceptional anharmonicity of the free-energy surfaces [8], a feature believed to be related to the nature of the Pb-O bond in these lead oxide solid solutions [34].

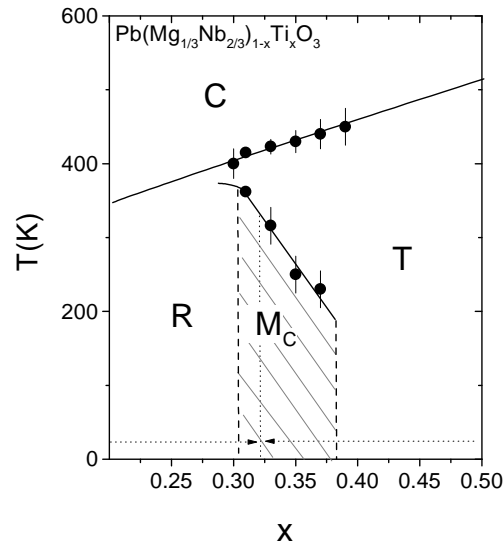


FIG. 10: Modified phase diagram of PMN-xPT around the MPB. The solid line indicating the transition to the cubic phase is the average of the two temperatures reported by Noblanc et al.[19] from dielectric measurements. The symbols separating the M_C and T phases represent the start of the M_C-T phase transition in those cases in which the sample volume has been found to transform gradually with temperature ($x=0.35, 0.37$)

There is the question of whether the observed phase coexistence, R+M_C, T+M_C, or even T+M_C+O is an intrinsic feature of the PMN-xPT system. The previously-noted degree of compositional fluctuation might by itself explain the coexistence of M_C and R phases in 31PT, but not the coexistence of M_C and T over a much wider range. According to the eighth-order Devonshire expansion of the free energy [8], a phase transition between R and M_C cannot occur directly and is only possible *via* an O phase [35]. In this work, we have observed that 31PT is very close to orthorhombic, and it seems entirely plausible that compositions might be found between 30PT and 31PT which are truly orthorhombic, in which case the transition between R and M_C will indeed occur *via* the O phase.

Furthermore, according to the eighth-order theory[8], the M_C-T phase transition should be second-order, and no phase coexistence region should be observed. However, the O-T phase transition is first-order, and there-

fore the presence of an O phase could explain the wide region of M_C+T phase coexistence observed. In fact, the existence of a minority third O phase, similar to that found in 35PT cannot be necessarily ruled out in 31PT, 33PT and 37PT, although in these cases we are unable to resolve it from the monoclinic phase. On the other hand, it is also possible that the continuous character of the M_C -T transition may be changed by considering higher-orders in the free energy expansion [8], since the Landau conditions for second-order transitions that are fulfilled in this case are necessary but not sufficient [31]. This would be more in accordance with the fairly abrupt changes in the lattice parameters, in special the order parameter $\beta-90^\circ$, observed at the transition as a function of composition, and the M_C -T phase coexistence could be naturally explained.

To conclude, a new phase diagram for PMN-xPT has been proposed which delimits the the composition range of the M_C phase near the MPB. The existence of a secondary phase, either tetragonal or rhombohedral, has been found in all cases ($31\% \leq x \leq 37\%$). Moreover, the presence of a third minority orthorhombic phase, observed for 35PT, cannot be ruled out in the other monoclinic compositions, and could explain the observed phase coexistence of M_C and T. This complex landscape of phase mixtures, which is in agreement with the obser-

vations of Xu et al. for 33PT single crystals [23], cannot be explained simply by long-range compositional fluctuations in the sample and is believed to be an intrinsic feature of the PMN-xPT system. The evolution of the monoclinic lattice parameters as a function of composition shows that the M_C phase evolves from the O limit and approaches the T limit, indicating that the polarization rotates in the monoclinic (010) plane. However, the rotation appears to be discontinuous at both limits. The present results show that the MPB of the MPB system is characterized by multi-phase components and complex phase behavior. We hope that our observations will stimulate further experimental and theoretical work needed to clarify more precisely the nature of the MPB and its relationship to the electromechanical properties.

Acknowledgments

We would like to thank A. Bokov and M. Dong for their help in sample preparation and B. Burton for useful discussions. Financial support from the U.S. Department of Energy under contract No. DE-AC02-98CH10886 and U.S. Office of Naval Research Grant No. N00014-99-1-0738 is also gratefully acknowledged.

-
- [1] S.-E. Park, and T. R. Shrout, *J. Appl. Phys.* **82**, 1804 (1997).
 - [2] D. Viehland, A. Amin, and J.F. Li, *Appl. Phys. Lett.* **79**, 1006 (2001).
 - [3] B. Jaffe, W. R. Cook, and H. Jaffe, *Piezoelectric Ceramics* (Academic Press, London, 1971).
 - [4] J. Kuwata, K. Uchino, and S. Nomura, *Ferroelectrics* **37**, 579 (1981).
 - [5] T. Shrout, Z.P. Chang, N. Kim, and S. Markgraf, *Ferroelectric Letters*, **12**, 63 (1990).
 - [6] B. Noheda, J.A. Gonzalo, L.E. Cross, R. Guo, S.-E. Park, D.E. Cox and G. Shirane *Phys. Rev. B* **61**, 8687 (2000); B. Noheda, D.E. Cox, G. Shirane, J.A. Gonzalo, L.E. Cross, and S-E. Park, *Appl. Phys. Lett.* **74**, 2059 (1999).
 - [7] B. Noheda, D.E. Cox, G. Shirane. R. Guo, B. Jones and L.E. Cross, *Phys. Rev. B* **63**, 014103 (2001)
 - [8] D. Vanderbilt and M. H. Cohen, *Phys. Rev. B* **63**, 094108 (2001).
 - [9] R. Guo, L.E. Cross, S-E. Park, B. Noheda, D.E. Cox, and G. Shirane, *Phys. Rev. Lett.* **84**, 5423 (2000).
 - [10] L. Bellaiche, A. Garcia, and D. Vanderbilt, *Phys. Rev. Lett.* **84**, 5427 (2000).
 - [11] X.-H. Du, J. Zheng, U. Belengu, and K. Uchino, *Appl. Phys. Lett.* **72**, 2421 (1998)
 - [12] D.V. Taylor and D. Damjanovic, *Appl. Phys. Lett.* **76**, 1615 (2000).
 - [13] H. Fu, and R. E. Cohen, *Nature* **403**, 281 (2000).
 - [14] B. Noheda, D.E. Cox, G. Shirane, S-E. Park, L.E. Cross and Z. Zhong, *Phys. Rev. Lett.* **86**, 3891 (2001)
 - [15] K. Ohwada, K. Hirota, P. Rehrig, P.M. Gehring, B. Noheda, Y. Fujii, S-E. Park, and G. Shirane, *J. Phys. Soc. Japan* **70**, 2778 (2001).
 - [16] D.E. Cox, B. Noheda, G. Shirane, Y. Uesu, K. Fujishiro, and Y. Yamada. *Appl. Phys. Lett.* **79**, 400 (2001)
 - [17] D. La-Orauttapong, B. Noheda, Z.-G. Ye, P.M. Gehring, J. Toulouse, D.E. Cox and G. Shirane *Phys. Rev. B.* **65**, 144101 (2002)
 - [18] Y. Uesu, M. Matsuda, Y. Yamada, K. Fujishiro, D.E. Cox, B. Noheda, and G. Shirane, *J. Phys. Soc. Japan* (in press). e-print: cond-mat/0106552.
 - [19] O. Noblanc, P. Gaucher, G. Calvarin, *J. Appl. Phys.* **79**, 4291 (1996)
 - [20] Y. Lu, D.-Y. Jeong, Z.-Y. Cheng, Q.M. Zang, H.-S. Luo, Z.-W. Yin, and D. Viehland, *Appl. Phys. Lett.* **78**, 3109 (2001)
 - [21] Z.-G. Ye, B. Noheda, M. Dong, D.E. Cox, and G. Shirane, *Phys. Rev. B.* **64**, 184114 (2001)
 - [22] Z.-G. Ye and M. Dong, *J. Appl. Phys.* **87**, 2312 (2000)
 - [23] G. Xu, H. Luo, H. Xu, and Z. Yin, *Phys. Rev. B.* **64**, 020102 (2001).
 - [24] J.-M. Kiat, Y. Uesu, B. Dkhil, M.X. Matsuda, C. Malibert, and G. Calvarin, *Phys. Rev. B.* **65**, 064106 (2002)
 - [25] A. K. Singh and D. Pandey, *J. Phys.: Condens. Matter* **13**, L931 (2001)
 - [26] S. L. Swartz and T. R. Shrout, *Mater. Res. Bull.* **17**, 1245 (1982).
 - [27] L.W. Finger, D.E. Cox, and A.P. Jephcoat, *J. Appl. Crystallogr.* **27**, 892 (1994).
 - [28] G.K. Williamson and W.H. Hall, *Acta Metall.* **1**, 22 (1953)
 - [29] A.M. Glazer, S.A. Mabud, and R. Clarke, *Acta Cryst. B* **34**, 1060 (1978)

- [30] D. L. Corker, A.M. Glazer, R.W. Whatmore, A. Stalard, and F. Fauth, *J. Phys.: Condensed Matter* **1**, 6251 (1998).
- [31] L.D. Landau and E.M. Lifshitz, *Statistical Physics I*. (Pergamon Press, New York, 1980)
- [32] V.Y. Topolov, *Phys. Rev. B* **65**, 094207 (2002).
- [33] B.P. Burton and E. Cockayne, *Phys. Rev. B.* **60**, R12542 (1999)
- [34] J-M. Kiat, G. Baldinozzi, M. Dunlop, C. Malibert, B. Bkhil, C. Menoret, O. Masson, and M-T. Fernandez-Diaz, *J. Phys.:Condens. Matter* **12**, 8411 (2000).
- [35] This would also be possible via a M_A phase. A triclinic phase in between the M_A and M_C phase would be likely to exist in this case [8, 10].